BMC Medical Imaging

RESEARCH

Open Access

Can the apparent transverse relaxation rate ($R2^*$) evaluate the efficacy of concurrent chemoradiotherapy in locally advanced nasopharyngeal carcinoma? a preliminary experience

Xinhua Xu[1], Ming Chen[1*], Jin Zhang[1], Yunzhu Jiang[1], Hua Chao[1] and Jianfeng Zha[1]

Abstract

Background The use of the apparent transverse relaxation rate ($R2^*$) in nasopharyngeal carcinoma (NPC) has not been previously reported in the literature. The aim of this study was to investigate the role of the $R2^*$ value in evaluating response to concurrent chemoradiotherapy (CCRT) in patients with NPC.

Methods Forty-one patients with locoregionally advanced NPC confirmed by pathology were examined by blood oxygenation level-dependent (BOLD) magnetic resonance imaging (MRI) before and after CCRT, and conventional MRI was performed 3 months after the completion of CCRT. All patients were divided into a responding group (RG) and a nonresponding group (NRG), according to MRI findings 3 months after the end of treatment. The $R2^*$ values before ($R2^*_{preT}$) and after ($R2^*_{postT}$) CCRT and the $\Delta R2^*$ ($\Delta R2^*=R2^*_{postT}-R2^*_{preT}$) were calculated in the tumor.

Results Among the 41 patients, 26 were in the RG and 15 were in the NRG. There was no statistical difference in the $R2^*_{preT}$ between RG and NRG ($P=0.307$); however, there were significant differences in $R2^*_{postT}$ and $\Delta R2^*$ ($P<0.001$). The area under the curve of $R2^*_{postT}$ and $\Delta R2^*$ for predicting the therapeutic response of NPC was 0.897 and 0.954, respectively, with cutoff values of 40.95 and 5.50 Hz, respectively.

Conclusion The $R2^*$ value can be used as a potential imaging indicator to evaluate the therapeutic response of locoregionally advanced NPC.

Keywords Locoregionally advanced nasopharyngeal carcinoma, Concurrent chemoradiotherapy, Hypoxia, Apparent transverse relaxation rate, Magnetic resonance imaging

*Correspondence:
Ming Chen
chenming1445@sina.com
[1]Department of Radiology, Changzhou Cancer Hospital of Soochow University, 68 Honghe Road, Changzhou 213000, Jiangsu, PR China

Background

Over 60% of patients with nasopharyngeal carcinoma (NPC) exhibit a locoregionally advanced stage at first diagnosis [1]. Radiotherapy has become a vital treatment approach for locoregionally advanced NPC [2]; however, the 5-year survival rate of patients with locoregionally advanced NPC after radiotherapy is only 50–70% [3]. The main mechanism of function of radiotherapy is that the reactive oxygen species generated by radiation destroy cellular structures [4]. During tumor progression, the abnormal structure and function of blood vessels and tumor cell proliferation lead to an insufficient oxygen supply accompanied by changes in the cancer cell microenvironment, which makes tumors more aggressive [5]. Hypoxia facilitates resistance of tumors against radiation and drug-induced cell death [6], promotes cancer cell proliferation [7], and increases the possibility of recurrence, locoregional spread, and distant metastasis [6, 8]. Therefore, hypoxia-induced treatment resistance is a major cause of treatment failure [9], and it has become an important obstacle to NPC treatment [10, 11]. Establishing a noninvasive and dynamic monitoring method to predict and evaluate the efficacy of NPC treatment is crucial for precision treatment.

Dynamic contrast-enhanced magnetic resonance imaging (DCE-MRI) and diffusion-weighted imaging (DWI) are the commonly used functional MRI techniques to evaluate NPC [12–14]. DCE-MRI provides functional information on neovascularization, and DWI reflects the diffusion characteristics of water molecules. However, they have the disadvantage of being unable to assess changes in oxygenation within the tumor. Blood oxygenation level-dependent MRI (BOLD-MRI), a noninvasive functional MRI to detect the oxygenation level of hemoglobin, indirectly reflects the oxygenation status of tissues [15]. BOLD-MRI uses the difference in tissue susceptibility properties between oxyhemoglobin (diamagnetic) and deoxyhemoglobin (paramagnetic) to express the signal by employing a gradient echo sequence with multiple echo times (TEs) [16]. The apparent transverse relaxation rate ($R2^*$) is inversely correlated with the oxygenation level of the tissue [17], and has an approximately linear relationship with the partial pressure of oxygen [18, 19]. $R2^*$ values increase when tissue oxygenation levels decrease, and decrease when oxygenation levels increase [20]. Therefore, the $R2^*$ value can be used as an index to assess tissue hypoxia; specifically, the higher the $R2^*$ signal intensity, the more apparent the tissue hypoxia [21].

Recently, BOLD-MRI technology has become a research hotspot [22–24]. The feasibility of $R2^*$ values for evaluating tumor oxygenation status has been demonstrated in studies of breast [25, 26], cervical [22], prostate [19], and rectal cancers [27]. However, there are only few reports on the application of $R2^*$ in NPC to date. Since hypoxia is one of the independent risk factors for NPC and $R2^*$ values can reflect the oxygenation status near tumor blood vessels, we hypothesized that $R2^*$ values would be associated with the final tumor response in patients with NPC receiving concurrent chemoradiotherapy (CCRT). Therefore, this study aimed to investigate the feasibility of the $R2^*$ value in evaluating the efficacy of CCRT in patients with locoregionally advanced NPC.

Materials and methods

Patients

This study was approved by the ethics committee of our hospital (file number 2022 - SY −017), and all patients provided informed consent. Forty-one patients with biopsy-proven locoregionally advanced NPC between January 2020 and December 2021 were enrolled in this study. These patients received CCRT, and underwent MRI before and after CCRT.

The inclusion criteria were as follows: (i) biopsy-confirmed NPC that met the criteria of locoregionally advanced NPC at T1-4N2-3M0 according to the 8th edition of the American Joint Committee on Cancer (AJCC) staging criteria for head and neck tumors; and (ii) absence of invasive examination or anticancer treatment history.

The exclusion criteria were as follows: (i) previous chemotherapy and/or radiotherapy history; (ii) interruption of CCRT; (iii) contraindications to MRI examination; and (iv) images that did not meet the requirements of delineating the region of interest (ROI).

All patients received concurrent intensity-modulated radiotherapy and chemotherapy. According to the MRI findings, gross tumor volume (GTVnx) and cervical metastatic lymph node volume (GTVnd) were delineated. Clinical target volume 1 (CTV1) was GTVnx extended by 5–10 mm. Clinical target volume 2 (CTV2) included the potential invasion area of the tumors and the neck lymphatic drainage area requiring prophylactic irradiation. The planning target volume (PTV) was expanded by 3–5 mm in a three-dimensional direction based on the CTV. The prescribed doses to the PTV for GTVnx, GTVnd, CTV1, and CTV2 were 68–70 Gy, 64–68 Gy, 60 Gy, and 54 Gy, respectively. Five sessions per week for a total of 30 sessions were conducted, and all patients received DDP (80 mg/m^2) chemotherapy. A course of treatment was received every 3 weeks, and a total of 2–3 courses were required.

MRI protocol

All patients underwent examination on a 3.0 T MR scanner (UMR 780, United-Imaging Healthcare, Shanghai, China) with a 24-channel phased-array head-neck coil. Conventional unenhanced and enhanced MRI scans were performed before and after CCRT, as well as 3 months

after CCRT completion. BOLD-MRI was also performed before and after CCRT. The MRI scan parameters were as follows: (i) conventional MRI unenhanced scan with fast spin-echo sequence: axial T1-weighted image (T1WI): repetition time (TR)=550 ms, echo time (TE)=13 ms, slice thickness=5 mm, slice gap=1 mm, field of view (FOV)=230 mm × 256 mm, matrix=320×224, flip of angle=111°. Unenhanced axial T2-weighted image: TR=3014 ms, TE=79 ms, slice thickness=5 mm, slice gap=1 mm, FOV=230 mm × 230 mm, matrix=384×288, flip of angle=150°. Enhanced T1WI was performed using fat suppression and the remaining parameters were the same as those used in the unenhanced scan. The contrast agent (Gadopentetate dimeglumine injection, Guangdong Kangchen Pharmaceutical Co., LTD., China) at a 0.1 mmol/kg dose was injected intravenously through the median cubital vein with a high-pressure syringe at 2.0 mL/s, followed by 20mL 0.9% normal saline at the same flow rate. (ii) BOLD-MRI: a five echo multi-echo gradient echo sequence: axial: TR=1177.8 ms, TE=6.71 /13.42/20.13/26.84/33.55 ms, slice thickness=5 mm, slice gap=1 mm, FOV=360 mm × 270 mm, matrix=256×218, flip of angle=60°.

Image analysis and data measurement

After data acquisition, the BOLD-MRI images were transferred to a post-processing workstation. Data analysis was performed using software (uWS-MR, version R003; United-Imaging Medical) provided by the manufacturer. The software automatically generated color-coded maps of $R2^*$; the colors from blue to red represented the $R2^*$ values from low to high on $R2^*$ maps. Axial sections of the tumor on enhanced T1WI and $R2^*$ maps were chosen for imaging analysis. ROI was manually delineated along the margin of the mass on the largest section. The $R2^*$ values of the tumor before and within one week after the end of treatment ($R2^*_{preT}$ and $R2^*_{postT}$, respectively), and the $\Delta R2^*$ ($\Delta R2^* = R2^*_{postT} - R2^*_{preT}$), were used for analysis. To test the interobserver reproducibility, ROIs were drawn independently by two radiologists (observers 1 and 2) with 10 and 5 years of experience, respectively. If there was a good level of agreement, the value of observer 1 was used for statistical analysis.

Table 1 Clinical data and staging of patients in RG and NRG

	RG (n = 26)	NRG (n = 15)	t/x^2	*p*
Age	51.88 ± 11.74	52.73 ± 14.08	–0.207[#]	0.837
Sex			3.349[Δ]	0.067
Male	18	6		
Female	8	9		
AJCC-TNM stage			0.241[Δ]	0.887
I	5	2		
II	11	7		
IVa	10	6		

Data are reported as mean ± SD

[#]Independent-samples t-test; [Δ]Chi-squared test

RG, responding group; NRG, nonresponding group; AJCC, American Joint Committee on Cancer

Response evaluation

Tumor size was defined as the largest diameter of mass measured on axial- enhanced T1WI. The results of the MRI examination 3 months after the end of treatment show that the tumors were divided into a responding group (RG) and a nonresponding group (NRG), as assessed by the Response Evaluation Criteria in Solid Tumors (version 1.1) as follows: RG: complete response or partial response after treatment; NRG: progressive disease or stable disease after treatment.

Statistical analysis

The IBM SPSS software (version 26.0; SPSS Inc., Chicago, IL, USA) was used to conduct statistical analysis. Normally distributed data were represented as mean ± standard deviation, whereas non-normally distributed data were represented as median (interquartile range). The intraclass correlation coefficient (ICC) was used to compare the inter-observer agreement. The agreement was scored as excellent (ICC > 0.75), moderate (ICC = 0.50–0.75), or poor (ICC < 0.50). The chi-square test was used to analyze sex and AJCC-TNM stage. $R2^*_{preT}$, $R2^*_{postT}$, and $\Delta R2^*$ were compared between RG and NRG using independent samples t-test or Mann–Whitney U test depending on the normality of data distribution. The receiver operating characteristic curve (ROC) was used to analyze and calculate the area under the ROC curve (AUC), sensitivity, and specificity, using the MedCalc 15.6.1 software. The cutoffs of RG and NRG were obtained by calculating the Youden index (Youden index = sensitivity + specificity — 1). The Delong test was used to compare the differences in AUC between the two groups. $p < 0.05$ was considered statistically significant.

Results

Clinical features

Overall, 41 patients (24 male and 17 female) were enrolled in the study, with a mean age of 52.20 ± 12.48 years (26–78 years). Tumors were evaluated 3 months after the completion of CCRT, and 26 and 15 patients were in RG and NRG, respectively. Table 1 shows the age, sex, and AJCC-TNM (tumor, node, metastasis) stage characteristics of all patients.

Comparison of interobserver agreement

The inter-observer agreement of $R2^*$ values measured by observer 1 and observer 2 was excellent (ICC = 0.801, $p < 0.0001$).

Comparison of parameters between RG and NRG

Table 2 shows that $R2^*_{preT}$ was not significantly different between RG and NRG; however, $R2^*_{postT}$ and $\Delta R2^*$ were significantly different. After CCRT, the average $R2^*$ value decreased in NRG (Fig. 1) and increased in RG (Fig. 2).

Diagnostic performance of $R2^*$ values

The AUC of $R2^*_{postT}$ and $\Delta R2^*$ for predicting the therapeutic response of NPC were 0.897 and 0.954, respectively (Fig. 3), and the cutoffs were 40.95 Hz and 5.50 Hz, respectively (Table 3). There was no significant difference in AUC between $R2^*_{postT}$ and $\Delta R2^*$ ($Z=1.020$, $p=0.308$).

Discussion

The $R2^*$ value can reflect the tissue oxygenation level. When the tissue oxygenation level is reduced the deoxyhemoglobin content in the tissue increases, leading to rapid dephasing of regional spins, a decrease in $T2^*$ relaxation time, and an increase in $R2^*$ ($R2^* = 1 / T2^*$ relaxation time). Additionally, when the oxygenation level increases, the increase of oxyhemoglobin in the tissue has little or no effect on the homogeneity of the local magnetic field; therefore, the $T2^*$ value increases and the $R2^*$ value decreases [20]. Presently, research on the $R2^*$ value mainly focuses on body tumors, and the related research on head and neck cancer, especially NPC, is rare. Our preliminary results showed that the $R2^*$ value could reflect the oxygenation changes before and after CCRT, and the post-treatment $R2^*$ and $\Delta R2^*$ values could predict CCRT response in NPC. Thus, the $R2^*$ value may be a useful marker for evaluating and predicting CCRT efficacy in NPC, which can better guide doctors and help them choose the appropriate treatment.

Our study showed that baseline $R2^*$ values before NPC treatment did not predict treatment response. Presently, studies on tumor baseline $R2^*$ mainly focus on histological grade [28, 29], and there are no reports on the relationship between baseline $R2^*$ values and CCRT treatment response in patients with NPC. Kim et al. [22] suggested that there was no significant correlation between the $R2^*$ value before treatment and the volume shrinkage rate after treatment in cervical cancer. All cases in our study were squamous cell carcinoma, and the same pathological type may be one of the reasons why the baseline $R2^*$ value of NPC cannot predict the therapeutic response.

Our study showed that the $R2^*$ value after CCRT and the $\Delta R2^*$ value were significantly different. This result indicated that although the tumor response to treatment is not correlated with the baseline $R2^*$ value, it is correlated with the corresponding $R2^*$ value after treatment. The changes in $R2^*$ values before and after CCRT indirectly reflected the oxygenation status within the tumor. Studies have shown that hypoxia is an independent factor for treatment resistance and poor prognosis [30, 31]. We observed that the tumor $R2^*$ value after treatment increased in the RG whereas it decreased in the NRG, indicating that effective treatment aggravated tumor hypoxia. Galban et al. [32] suggested that local blood perfusion is rapidly reduced and tumor hypoxia is more severe during treatment, especially in the early stage. Studies have shown that $R2^*$ values are affected by multiple factors including oxyhemoglobin level, blood volume, and vascular distribution [28]. Increased $R2^*$ values are

Table 2 Comparison of parameters between RG and NRG

	RG (n = 26)	NRG (n = 15)	*t/U*	*p*
$R2^*_{preT}$ (Hz)	43.78 ± 12.00	48.02 ± 13.69	−1.034$^{\Delta}$	0.307
$R2^*_{postT}$ (Hz)	58.23 ± 12.13	37.83 ± 9.62	5.595$^{\Delta}$	< 0.001
$\Delta R2^*$ (Hz)	16.10 (20.6–12.43)	−10.19 ± 7.57	372$^{\#}$	< 0.001

$^{\Delta}$Independent-samples t-test (data are reported as mean ± SD); $^{\#}$Mann–Whitney U test (data are reported as median (3rd quartile–1st quartile)

RG, responding group; NRG, nonresponding group; $R2^*_{preT}$, $R2^*$ value of tumor before CCRT; $R2^*_{postT}$, $R2^*$ value of tumor after CCRT; $\Delta R2^*$, $R2^*_{postT} - R2^*_{preT}$; CCRT, concurrent chemoradiotherapy

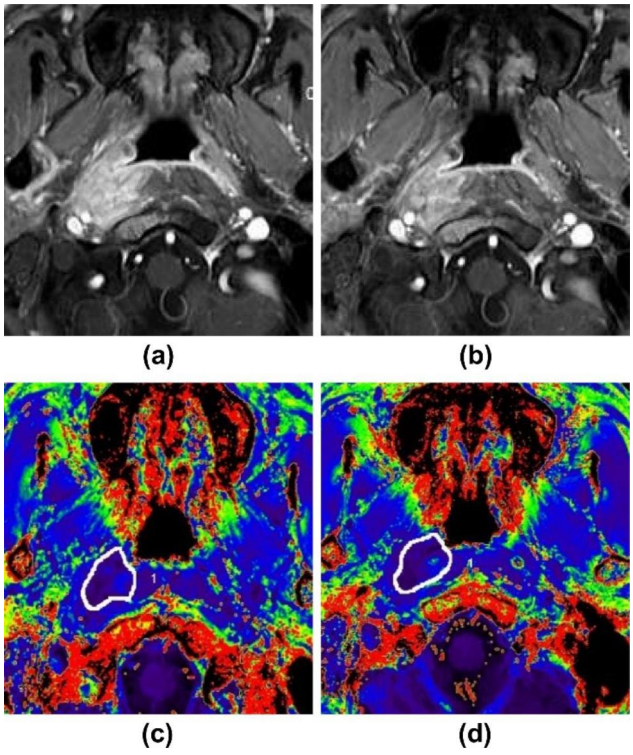

Fig. 1 A young man with nasopharyngeal carcinoma (AJCC stage III). **(a)** Axial enhanced fat suppression T1WI before CCRT with lesions located on the right side. **(b)** Axial enhanced fat suppression T1WI at 3 months after the end of CCRT indicates stable disease (SD) according to RECIST 1.1; the patient was included in NRG. **(c)** $R2^*$ value in the ROI was 36.40 Hz on the $R2^*$ color-coded map before CCRT. **(d)** $R2^*$ value in the ROI was 34.70 Hz at 3 months after the end of CCRT. CCRT, concurrent chemoradiotherapy; RECIST, response evaluation criteria for solid tumors; NRG, nonresponding group; ROI, region of interest' AJCC, American Joint Committee on Cancer; T1WI, T1-weighted image

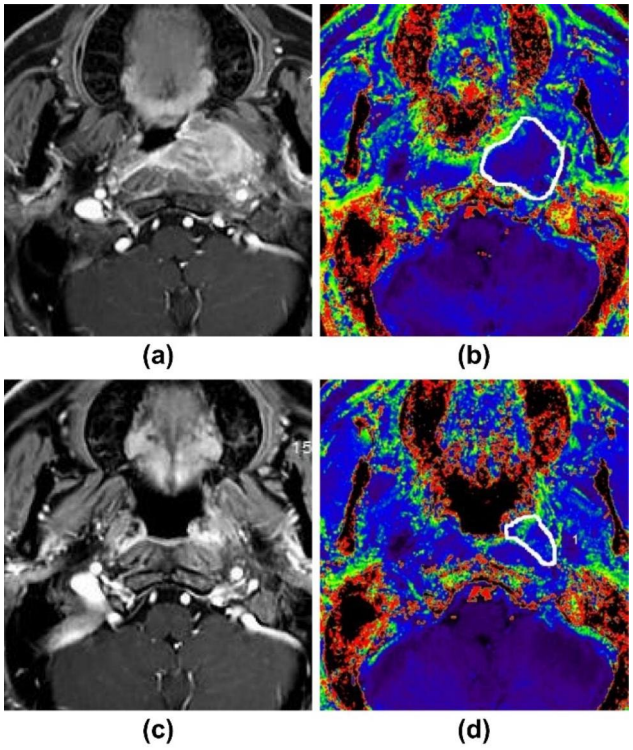

Fig. 2 An elderly man with nasopharyngeal carcinoma (AJCC stage III). **(a)** Axial enhanced fat suppression T1WI before CCRT with lesions located on the left side. **(b)** Axial enhanced fat suppression T1WI at 3 months after the end of CCRT indicates a partial response (PR) according to RECIST 1.1; the patient was included in RG. **(c)** $R2^*$ value in the ROI was 45.90 Hz on the $R2^*$ color-coded map before CCRT. **(d)** $R2^*$ value in the ROI was 66.40 Hz at 3 months after the end of CCRT. CCRT, concurrent chemoradiotherapy; RECIST, response evaluation criteria for solid tumors; RG, responding group; ROI, region of interest; AJCC, American Joint Committee on Cancer; T1WI, T1-weighted image

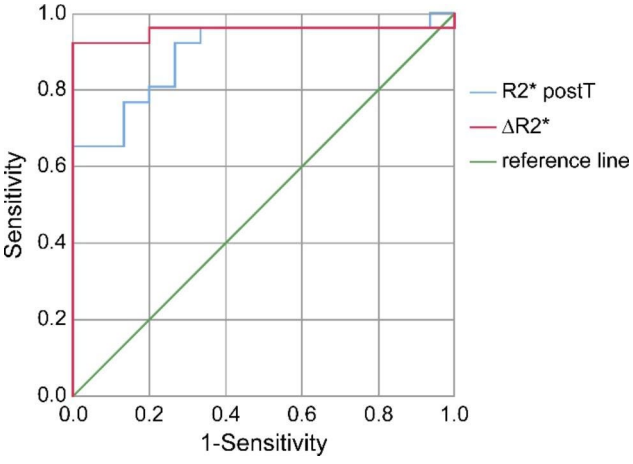

Fig. 3 The area under the ROC curve on $R2^*_{postT}$ and $\Delta R2^*$ for differentiating the therapeutic response to CCRT. ROC, receiver operating characteristic; CCRT, concurrent chemoradiotherapy

most commonly due to an increase in the paramagnetic iron content of deoxyhemoglobin, and reduced $R2^*$ values are often attributed to calcification or edema [33]. We speculate that effective radiotherapy and chemotherapy destroy the endothelial cells of tumor vessels, increase vascular permeability, and allow soluble oxygen in oxygenated hemoglobin to diffuse between the perfused blood vessels and adjacent tissues, thereby resulting in an increase in the content of paramagnetic deoxyhemoglobin in the tumor blood vessels. Concurrently, ferroptosis of hypoxic tumor cells caused by radiotherapy also increases blood iron content, leading to the increase of the $R2^*$ value. There was little change in oxyhemoglobin and deoxyhemoglobin levels in treatment-insensitive tumor tissue; thus, there was little change in the homogeneity of the local magnetic field [20]. The decrease in $R2^*$ value may be related to tissue edema caused by radiotherapy. Our study showed that the AUC of $R2^*_{postT}$ and $\Delta R2^*$ for predicting therapeutic response were 0.897 and 0.954, respectively. The cutoffs of $R2^*_{postT}$ and $\Delta R2^*$ for predicting response were 40.95 Hz and 5.50 Hz, respectively, with a sensitivity of 92.3% and specificity of 73.3% and 100%, respectively. This finding suggests that $R2^*$ values can be measured immediately after CCRT in NPC cases to predict therapeutic response. Hence, treatment strategies can be adjusted early based on the $R2^*$ value, whereas conventional MRI evaluation typically requires 3 months after the end of treatment.

Our study has some limitations that should be acknowledged. First, this was a preliminary study, and the evaluated technique was not compared with other MRI techniques. In the future, it is necessary to combine DCE-MRI, DW-MRI, and other techniques to verify the true role of the $R2^*$ value as a potential biomarker in evaluating treatment efficacy in NPC. Second, there is a lack of pathological evidence due to the unresectable nature of NPC. Since the changes in tumor microstructure precede the changes in imaging, it cannot be ignored that some patients with effective treatment may be misclassified as NRG. Finally, small lesions on the nasopharyngeal surface may affect the accuracy of $R2^*$ measurements because of artifacts caused by air-tissue interfaces.

Conclusions

This study demonstrated that the $R2^*$ value at the end of CCRT may predict the treatment response at 3 months after CCRT in locoregionally advanced NPC. Compared with the assessment based on morphological changes, the $R2^*$ value can accurately assess the oxygenation status of locoregionally advanced NPC during treatment and can provide a new treatment strategy.

Table 3 Diagnostic efficacy of $R2^*_{postT}$ and $\Delta R2^*$ for predicting therapeutic response to CCRT

	AUC	95%CI	Cutoff	Sensitivity (%)	Specificity (%)
$R2^*_{postT}$ (Hz)	0.897	0.800–0.995	40.95	92.3	73.3
$\Delta R2^*$ (Hz)	0.954	0.878–1.000	5.50	92.3	100.00

AUC, area under the curve; 95% CI, 95% confidence interval. CCRT, concurrent chemoradiotherapy

Abbreviations

NPC	nasopharyngeal carcinoma
BOLD	blood oxygen level-dependent
MRI	magnetic resonance imaging
CCRT	concurrent chemoradiotherapy
RG	responding group
NRG	nonresponding group
$R2^*$	apparent transverse relaxation rate
$R2^*_{preT}$	$R2^*$ value of tumor before CCRT
$R2^*_{post}$	$R2^*$ value of tumor after CCRT
DWI	diffusion-weighted imaging
DCE	dynamic contrast-enhanced
ICC	intraclass correlation coefficient
AJCC	American Joint Committee on Cancer
TE	echo time
GTVnx	gross tumor volume
GTVnd	cervical metastatic lymph node volume
CTV 1	clinical target volume 1
CTV2	clinical target volume 2
PTV	planning target volume
T1WI	T1-weighted image
TR	repetition time
FOV	field of view
ROI	region of interest
ICC	intraclass correlation coefficient
ROC	receiver operating characteristic curve
AUC	area under the ROC curve

Acknowledgements
We would like to thank Editage (www.editage.cn) for English language editing.

Author's contributions
XHX contributed to the investigation and writing of the initial manuscript. MC contributed to conceptualization, funding acquisition, and manuscript revision. JZ contributed to conceptualization. YZJ contributed to the data analysis. HC and JFZ contributed to the investigation. All authors reviewed and approved the final manuscript.

Funding
This study was supported by Changzhou Sci & Tech Program (Grant No. CJ20210169). The funding body played no role in the design of the study and collection, analysis, interpretation of data, and in writing the manuscript.

Data Availability
The datasets generated and analyzed during the current study are not publicly available because they contain information that could compromise the privacy of the research participants, but they will be available from the corresponding author on reasonable request.

Declarations

Ethics approval and consent to participate
This study was approved by the ethics committee of Changzhou Cancer Hospital of Soochow University (No. 2022-SY-017). All patients provided written informed consent for participation in this study. All procedures were conducted in accordance with guidelines and regulations laid down by the Institutional Review Board.

Consent for publication
Not applicable.

Competing interests
The authors declare that they have no competing interests.

Received: 25 January 2023 / Accepted: 23 May 2023
Published online: 01 June 2023

References

1. Bray F, Ferlay J, Soerjomataram I, Siegel RL, Torre LA, Jemal A. Global cancer statistics 2018: GLOBOCAN estimates of incidence and mortality worldwide for 36 cancers in 185 countries. CA Cancer J Clin. 2018;68:394–424.
2. Chen YP, Ismaila N, Chua MLK, Colevas AD, Haddad R, Huang SH, et al. Chemotherapy in combination with radiotherapy for definitive-intent treatment of stage II-IVA nasopharyngeal carcinoma: CSCO and ASCO Guideline. J Clin Oncol. 2021;39:840–59.
3. Mao YP, Tang LL, Chen L, Sun Y, Qi ZY, Zhou GQ, et al. Prognostic factors and failure patterns in non-metastatic nasopharyngeal carcinoma after intensity-modulated radiotherapy. Chin J Cancer. 2016;35:103.
4. Graham K, Unger E. Overcoming tumor hypoxia as a barrier to radiotherapy, chemotherapy and immunotherapy in cancer treatment. Int J Nanomedicine. 2018;13:6049–58.
5. Vaupel P, Kallinowski F, Okunieff P. Blood flow, oxygen and nutrient supply, and metabolic microenvironment of human tumors: a review. Cancer Res. 1989;49:6449–65.
6. Padhani AR, Krohn KA, Lewis JS, Alber M. Imaging oxygenation of human tumours. Eur Radiol. 2007;17:861–72.
7. Yin H, Qiu X, Shan Y, You B, Xie L, Zhang P, et al. HIF-1alpha downregulation of mir-433-3p in adipocyte-derived exosomes contributes to NPC progression via targeting SCD1. Cancer Sci. 2021;112:1457–70.
8. Vaupel P. The role of hypoxia-induced factors in tumor progression. Oncologist. 2004;9;Suppl 5:10 – 7.
9. Rottey S, Madani I, Deron P, Van Belle S. Modern treatment for nasopharyngeal carcinoma: current status and prospects. Curr Opin Oncol. 2011;23:254–8.
10. Lu J, Tang M, Li H, Xu Z, Weng X, Li J, et al. EBV-LMP1 suppresses the DNA damage response through DNA-PK/AMPK signaling to promote radioresistance in nasopharyngeal carcinoma. Cancer Lett. 2016;380:191–200.
11. Vaupel P, Mayer A. Tumor hypoxia: causative mechanisms, microregional heterogeneities, and the role of tissue-based hypoxia markers. Adv Exp Med Biol. 2016;923:77–86.
12. Lee MK, Choi Y, Jung SL. Diffusion-weighted MRI for predicting treatment response in patients with nasopharyngeal carcinoma: a systematic review and meta-analysis. Sci Rep. 2021;11:18986.
13. Zhao DW, Fan WJ, Meng LL, Luo YR, Wei J, Liu K, et al. Comparison of the pre-treatment functional MRI metrics' efficacy in predicting locoregionally advanced nasopharyngeal carcinoma response to induction chemotherapy. Cancer Imaging. 2021;21:59.
14. Mui AWL, Lee AWM, Lee VHF, Ng WT, Vardhanabhuti V, Man SSY, et al. Prognostic and therapeutic evaluation of nasopharyngeal carcinoma by dynamic contrast-enhanced (DCE), diffusion-weighted (DW) magnetic resonance imaging (MRI) and magnetic resonance spectroscopy (MRS). Magn Reson Imaging. 2021;83:50–6.
15. Wakefield JC, Downey K, Kyriazi S, DeSouza NM. New MR techniques in gynecologic cancer. AJR Am J Roentgenol. 2013;200:249–60.
16. Chaudhry AA, Naim S, Gul M, Chaudhry A, Chen M, Jandial R, et al. Utility of preoperative blood-oxygen-level-dependent functional MR imaging in patients with a central nervous system neoplasm. Neuroimaging Clin N Am. 2021;31:93–102.
17. Prasad PV. Evaluation of intra-renal oxygenation by BOLD MRI. Nephron Clin Pract. 2006;103:c58–65.
18. Inoue T, Kozawa E, Okada H, Inukai K, Watanabe S, Kikuta T, et al. Noninvasive evaluation of kidney hypoxia and fibrosis using magnetic resonance imaging. J Am Soc Nephrol. 2011;22:1429–34.

19. Luttje MP, van Buuren LD, Luijten PR, van Vulpen M, van der Heide UA, Klomp DWJ. Towards intrinsic R2* imaging in the prostate at 3 and 7tesla. Magn Reson Imaging. 2017;42:16–21.
20. Conklin CJ, Middleton DM, Mohamed FB. Fundamentals of preoperative task functional brain mapping. Top Magn Reson Imaging. 2019;28:205–12.
21. Hall ME, Jordan JH, Juncos LA, Hundley WG, Hall JE. BOLD magnetic resonance imaging in nephrology. Int J Nephrol Renovasc Dis. 2018;11:103–12.
22. Kim CK, Park SY, Park BK, Park W, Huh SJ. Blood oxygenation level-dependent MR imaging as a predictor of therapeutic response to concurrent chemoradiotherapy in cervical cancer: a preliminary experience. Eur Radiol. 2014;24:1514–20.
23. Chen J, Chen Q, Zhang J, Pan L, Zha T, Zhang Y, et al. Value of T2 mapping in the dynamic evaluation of renal ischemia-reperfusion injury. Acad Radiol. 2022;29:376–81.
24. O'Connor JPB, Robinson SP, Waterton JC. Imaging tumour hypoxia with oxygen-enhanced MRI and BOLD MRI. Br J Radiol. 2019;92:20180642.
25. Seo M, Ryu JK, Jahng GH, Sohn YM, Rhee SJ, Oh JH, et al. Estimation of T2* relaxation time of breast cancer: correlation with clinical, imaging and pathological features. Korean J Radiol. 2017;18:238–48.
26. Wang Y, Liu M, Jin ML. Blood oxygenation level-dependent magnetic resonance imaging of breast cancer: correlation with carbonic anhydrase IX and vascular endothelial growth factor. Chin Med J (Engl). 2017;130:71–6.
27. Ge YX, Hu SD, Wang Z, Guan RP, Zhou XY, Gao QZ, et al. Feasibility and reproducibility of T2 mapping and DWI for identifying malignant lymph nodes in rectal cancer. Eur Radiol. 2021;31:3347–54.
28. Wang Y, Shen Y, Hu X, Li Z, Feng C, Hu D, et al. Application of R2* and apparent diffusion coefficient in estimating tumor grade and T category of bladder cancer. AJR Am J Roentgenol. 2020;214:383–9.
29. Peng Y, Luo Y, Hu X, Shen Y, Hu D, Li Z, et al. Quantitative T2*-weighted imaging and reduced field-of-view diffusion-weighted imaging of rectal cancer: correlation of R2* and apparent diffusion coefficient with histopathological prognostic factors. Front Oncol. 2021;11:670156.
30. van der Heijden M, de Jong MC, Verhagen CVM, de Roest RH, Sanduleanu S, Hoebers F, et al. Acute hypoxia profile is a stronger prognostic factor than chronic hypoxia in advanced stage head and neck cancer patients. Cancers (Basel). 2019;11:583.
31. Zandberg DP, Menk AV, Velez M, Normolle D, Depeaux K, Liu A, et al. Tumor hypoxia is associated with resistance to PD-1 blockade in squamous cell carcinoma of the head and neck. J Immunother Cancer. 2021;9:e002088.
32. Galbán CJ, Chenevert TL, Meyer CR, Tsien C, Lawrence TS, Hamstra DA, et al. The parametric response map is an imaging biomarker for early cancer treatment outcome. Nat Med. 2009;15:572–6.
33. Belliveau JG, Bauman GS, Macdonald D, Macdonald M, Klassen LM, Menon RS. Apparent transverse relaxation (R2*) on MRI as a method to differentiate treatment effect (pseudoprogression) versus progressive disease in chemoradiation for malignant glioma. J Med Imaging Radiat Oncol. 2018;62:224–31.

Publisher's Note